2020 SNMMI Highlights Lecture: General Nuclear Medicine and Molecular Imaging

Heather A. Jacene, MD, Dana-Farber Cancer Institute, Brigham and Women's Hospital, and Harvard Medical School, Boston, MA

From the Newsline Editor: The Highlights Lecture, presented at the closing session of each SNMMI Annual Meeting, was originated and presented for more than 30 years by Henry N. Wagner, Jr., MD. Beginning in 2010, the duties of summarizing selected significant presentations at the meeting were divided annually among 4 distinguished nuclear and molecular medicine subject matter experts. Each year Newsline publishes these lectures and selected images. The 2020 Highlights Lectures were delivered on July 14 as part of the SNMMI Virtual Annual Meeting. In this issue we feature the lecture by Heather A. Jacene, MD, associate professor in the Department of Radiology at the Dana-Farber Cancer Institute, Brigham and Women's Hospital, and Harvard Medical School (Boston, MA), who spoke on highlights in general nuclear and molecular imaging. Note that in the following presentation summary, numerals in brackets represent abstract numbers as published in The Journal of Nuclear Medicine *(2020;61[suppl 1]).*

It is a delight to present the General Nuclear Medicine highlights for this virtual 2020 SNMMI Annual Meeting. This year, there were 135 abstracts (79 accepted as oral presentations and 56 as posters) presented in the General Clinical Nuclear Medicine track, covering musculoskeletal (18), gastroenterology (10), renal (14), pediatric (13), infectious disease (23), and nontherapy endocrinology (57) topics in 10 oral and 6 poster sessions. Abstract submissions again came from around the world, with the United States (57) and China (23) having the highest number, followed by India (12), Japan (7), and Canada (5), with many other countries represented. I thank everyone who sent slides for this presentation and regret that time limitations prevent sharing all of the excellent work presented at this year's meeting. In this year's unusual virtual format, I missed the face-to-face encounters at oral and poster sessions and opportunities to discuss research with authors but am encouraged by the exciting and innovative work presented.

Many of the abstracts this year hit on multiple and sometimes overlapping themes, and it was challenging to group them for this summary. I decided on 2 major categories—protocol optimization and tracer development—both of which also touch on image quality and time efficiency. Abstracts focused on new software and hardware were also related to time efficiency.

Protocol Optimization

Although ^{18}F-FDG PET/CT is used today in many instances to interrogate for infection, multiple indications remain for radiolabeled leukocyte scanning. Bhargava et al. from the Zucker School of Medicine at Hofstra Northwell (Hempstead, NY), Long Island Jewish Medical Center (New Hyde Park, NY), and MicroMedicine, Inc. (Waltham, MA) reported on "Labeled leukocyte imaging: Improved leukocyte isolation with a novel automated microfluidics-based system" [541]. Microfluidic leukocyte isolation is accomplished through a series of microchannels and microstructures that fractionate blood components. This reduces the number of radiolabeled red blood cells and platelets in the final injectate and should reduce the background blood pool appearance of the images we are accustomed to seeing. In this prospective study, 19 patients had 80 cc of whole blood withdrawn. Forty cc were sent for conventional radiolabeling and 40 cc for microfluidic isolation radiolabeling with ^{111}In-oxine (8 patients) or ^{99m}Tc-exametazime (11 patients), respectively. Superior results were found for the novel microfluidic approach. There was greater purity of the isolate from the microfluidic approach. The microfluidic technique had a shorter processing time of $<$40 minutes, compared to $>$110 minutes for the conventional technique. Greater radiolabel stability was seen for both radionuclides, with no difference between the techniques for labeling efficiency or leukocyte viability. In addition to improved image quality from purer leukocyte isolates, better isolation methods may also be of benefit in patients with low white blood cell counts, where our ability to use white blood cell imaging is limited. This research team is planning the next phase of investigation, comparing imaging results using conventionally isolated vs. microfluid-isolated white blood cells in patients with suspected arthroplasty infections.

Heather A. Jacene, MD

For evaluation of chronic cholecystitis and determining gallbladder ejection fraction (GBEF), current guidelines support 60-minute sincalide-stimulated cholescintigraphy, with a GBEF $>$38% considered as normal. Vasireddi et al. from the University of Pittsburgh/University of Pittsburgh Medical Center (PA) reported on "Sincalide-stimulated cholescintigraphy: A retrospective study and proposal of a modified workflow" [421]. They hypothesized that most subjects with a normal GBEF will achieve a normal EF by 30 minutes; if true, a shorter workflow could be implemented. The retrospective study included 302 patients, with GBEFs at 20 and 30 minutes estimated manually from time–activity curves generated at the time of the examinations. About 12% of patients (36) had abnormal GBEFs ($\leq$38%) representing chronic cholecystitis. Of the 88% (266

patients) with normal GBEFs at 60 minutes, 61% (163 patients) achieved a normal GBEF (>38%) at 20 minutes, and this increased to about 88% (233 patients) at 30 minutes. These findings agreed with the authors' hypothesis. Based on these results they proposed a new workflow, performing dynamic imaging in two 30-minute sections, stopping for a normal EF (>38%) at 30 minutes, continuing if abnormal at that time point, and then combining both sections to calculate the final GBEF. This has the potential to be time saving, particularly with experienced technical staff and physicians to gauge a normal GBEF at 30 minutes. What might be extremely important in implementing this modification on a larger scale would be the real-time ability to draw a region of interest on the gallbladder in the first 10 minutes of the study and then watch it dynamically to make the most accurate decision at the 30-minute time point. This is a challenge for software development teams in the field.

Protocol Optimization: Software/Hardware

Emerging data over the past several years support the continued investigation of ways in which the use of SPECT/CT techniques can lead to improvements in presurgical lobar lung quantification. One of the continuing challenges is accurate segmentation of the lung lobes. Performed manually, this can be quite time consuming and limits consistent comparison and widespread implementation. This is a promising area for application of artificial intelligence in general nuclear medicine. Gao and colleagues from Siemens Medical Solutions (Knoxville, TN, and Hoffman Estates, IL), Siemens Healthcare GmbH (Erlangen and Forchheim, Germany), Siemens Healthineers (Princeton, NJ), and University Hospital Basel (Switzerland) reported on "Evaluation of automatic lung lobe segmentation for SPECT/CT lung V/Q image analysis" [1489]. They evaluated the performance of an automated image analysis workflow on datasets from 15 patients with abnormal anatomy or images with limited lung fissure visibility from lower-dose CT acquisitions. In Figure 1, the top row shows the steps used for data input, landmark detection from CT, and application of a deep image-to-image network for the automated workflow to generate visualization of the lung segments and then 3D SPECT quantification. The bottom row shows 2 examples in which the automated workflow was able to identify abnormal anatomy. On the left, a smaller right superior lobe was observed in a patient with an enlarged lung as the result of emphysema. On the right, segmentation around a right upper lobe lung mass clearly differentiated the tumor. For comparison to this automated workflow, 1 nuclear medicine reader also manually performed the segmentation. The physician performing the manual segmentation then assigned the manual and automated study results into 2 groups: 1 in which there was sufficient delineation of lung fissures and a second in which there was not. A second nuclear medicine physician then graded the quality of the segmentation on a scale of 1–10 (10 being the best). In group 1, the quality of the segmentation was the same for manual and automatic segmentation. For group 2, the automated method received reasonable quality scores but not as good as the manual segmentation. When the manual and automated techniques in both groups 1 and 2 were compared quantitatively using the Dice score, segmentation results were overlapping. Most important, the automated workflow completed lung lobe segmentation successfully and generated results in <30 seconds per patient. So even in those challenging cases in which a reader needs to make manual adjust-

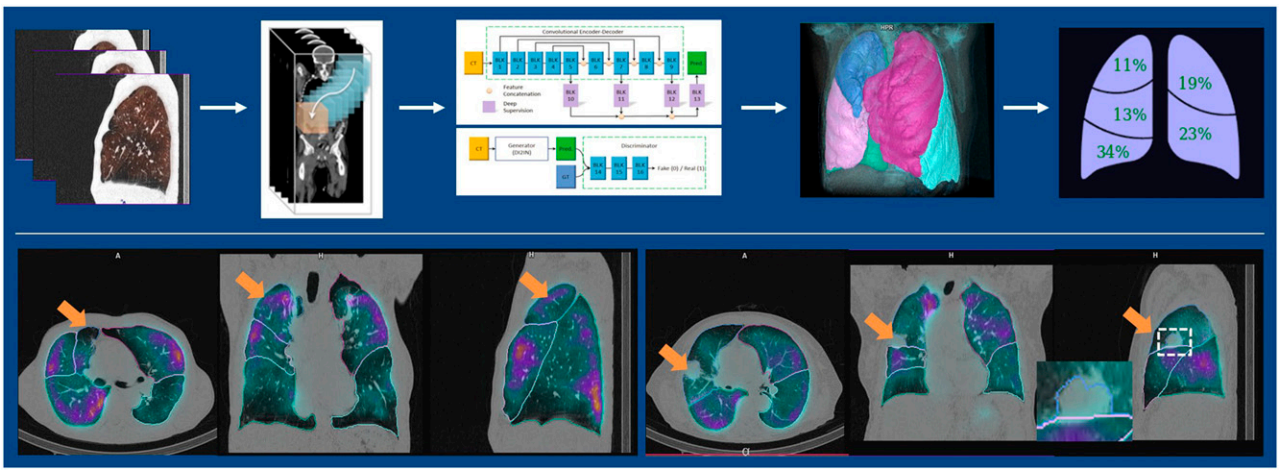

FIGURE 1. Automatic lung V/Q analysis workflow (top row, left to right): SPECT/CT volume data input, landmark detection from CT, application of a deep image-to-image network for automated workflow, resulting visualization of lung segments, and 3D SPECT quantification. Bottom: Examples of automated workflow identification of abnormal anatomy. Left block: Imaging in enlarged lung as a result of emphysema; automated workflow detected smaller right superior lobe (arrows). Right block: Segmentation around a right upper lobe lung mass clearly differentiated tumor. Automated workflow completed lung lobe segmentation successfully and generated results in <30 seconds per patient.

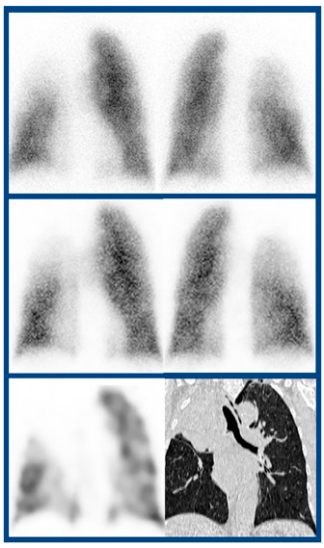

FIGURE 2. Multiview planar imaging with 360° whole-body CZT camera for presurgical assessment of lung cancer. Top block: Anterior and posterior planar images obtained with an Anger camera. Middle block: Anterior and posterior multiview planar images in the same patient. Bottom block: Coronal and low-dose CT data acquired with the multiview camera. Excellent correlation was found with conventional planar imaging for both the multiview planar and associated 3D SPECT/CT images (r^2 = 0.94 and 0.99, respectively).

ments, the time saved from such an automated workflow could be extremely valuable. Other groups are also working on similar segmentation models for lung imaging.

Several presenters at the meeting described the use of whole-body 360° cadmium-zinc-telluride (CZT) cameras and compared results with those from traditional planar imaging. Acquisition protocols with this CZT camera can be as short as 5 minutes and can generate both SPECT/CT images and reconstructed planar projections, a combination called "multiview planar" imaging. Melki et al. from the Centre Hospitalier Régional Universitaire–Nancy (Vandoeuvre-lès-Nancy, France) reported on "Assessment of multiview planar imaging provided by a high-speed 360° whole-body CZT camera in patients undergoing presurgical assessment of a lung cancer" [1488]. In this study, 20 consecutive patients undergoing presurgical assessment underwent conventional planar imaging and a CZT SPECT/CT acquisition. In an example set of images (Fig. 2), the quality and areas of abnormality in the right upper lobe of the lung appear similar between the planar and multiview planar images. One might argue that the resolution is slightly better in the multiview planar images than in those obtained with the Anger camera. Additional information is available from the SPECT/CT slices. Excellent correlation for differential lung function was seen between conventional planar and CZT SPECT/CT images (r^2 = 0.99 for 3D SPECT/CT and r^2 = 0.94 for multiview planar).

Bahloul et al., also from the Centre Hospitalier Régional Universitaire–Nancy, reported on "Dimercaptosuccinic acid (DMSA) renal investigations performed with a 360° whole-body CZT SPECT camera as compared with the conventional method based on planar images from an Anger camera" [244]. In this study, 21 consecutive patients (age range. 6 months–85 years) underwent ^{99m}Tc-DMSA scanning with a conventional Anger camera and the CZT camera. The CZT camera acquisition time was about 5 minutes. The count rate detected by the CZT camera was 180% of that with the conventional camera. Interpretations were concordant in 90% of paired image sets from the 2 cameras. The 2 discordant cases are shown in Figure 3 and were ultimately considered as having a more accurate diagnosis from the CZT camera. In the top images, a small defect not called on the planar images was visible with the CZT SPECT camera. In the bottom images, a small defect was called as a false-positive on the planar image but was shown to have contiguous cortical uptake of tracer with the CZT SPECT camera. Excellent correlation was also seen between relative kidney function with both acquisitions (r^2 = 0.98). The CZT SPECT camera technology has multiple potential advantages, including shorter acquisition times to enhance workflow, additional benefits of shorter acquisition time in reducing patient motion and improving image quality, the ability to have both SPECT/CT and planar reconstructions in a single acquisition, and the potential for reduced administered activity because of higher count rate detection.

Protocol Optimization: Bowel Transit

One theme of reports presented this year pertaining to protocol optimization related to bowel transit studies; a topic that is rarely covered in these highlights sessions. I did a quick survey of colleagues from around the country, in both academia and private practice, in preparation for this talk. Their average number of gastric emptying studies per week varied between 10 and 20, so work relating to optimization and understanding of these protocols remains relevant in general nuclear medicine practice.

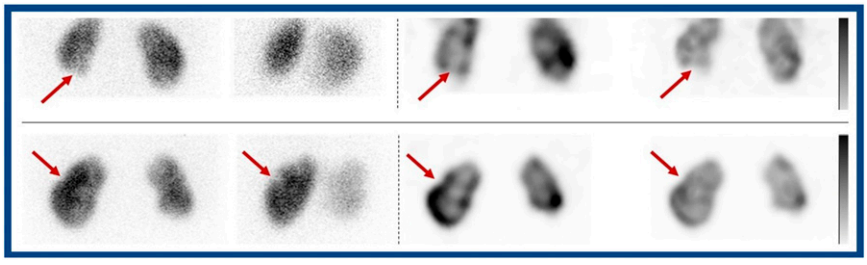

FIGURE 3. ^{99m}Tc-DMSA multiplanar view renal imaging with a whole-body CZT camera (right pairs in each set of images) vs. conventional Anger camera planar imaging (left pairs in each set of images). Although 90% of interpretations with these 2 methods were concordant in this study, these 2 were discordant. In patient 1 (top row), conventional imaging was found to be false-negative, whereas the CZT SPECT was true-positive, identifying a small cortical defect in the right inferior kidney. In patient 2 (bottom row), conventional imaging called a small defect as positive, whereas CZT SPECT correctly showed contiguous cortical uptake of the tracer. CZT camera acquisition time was about 5 minutes, with a count rate detection 180% of that with the conventional camera.

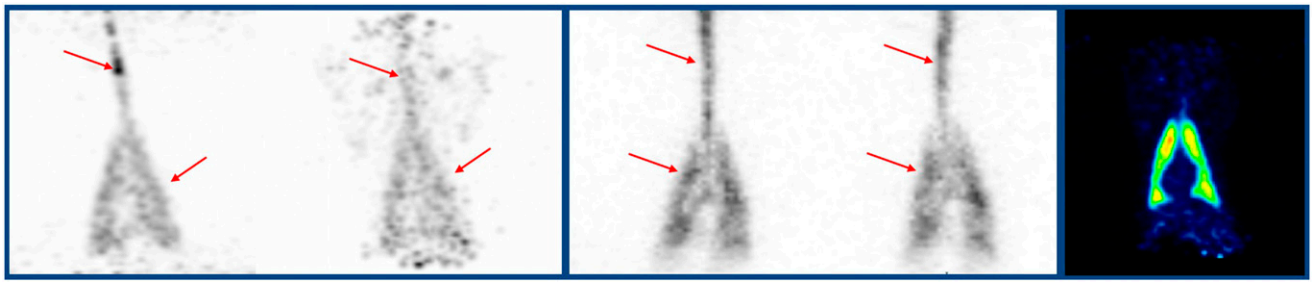

FIGURE 4. Radioaerosolized ^{18}F-fluoride-alumina nanoparticle imaging of mucociliary transport and clearance in a ferret model of cystic fibrosis. Images show ^{18}F-fluoride-alumina nanoparticle (left) and ^{99m}Tc-sulfur colloid (middle) clearance at trachea and upper/lower lobes of lung at 5 and 60 minutes after administration. Right: Early dynamic PET/CT at 5 minutes showed ^{18}F-fluoride-alumina nanoparticle activity deposition in lungs. The ultimate goal of this research is to translate the imaging technique to patients with cystic fibrosis, particularly for monitoring response to therapy.

Although gastric emptying studies are routinely performed in pediatric patients, no normal values exist for this population. At the same time, studies have shown that up to 70% of children may not be able to tolerate the complete standard meal or may require an alternate meal. Ng et al. from the Brigham and Women's Hospital, Brandeis University, and Boston Children's Hospital (all in Boston, MA) asked "How much do we need to eat? Assessment of partial standard and alternative meals for use in pediatric gastric emptying studies" [117]. In a second report, they described "Assessment of nonstandard cheese-based meals as viable alternatives to the standard adult meal for pediatric gastric emptying scintigraphy" [1580]. They performed a retrospective review of >1,000 studies to assess the applicability of the adult standard meal criterion of <10% meal retention by 4 hours after meal ingestion for partially consumed adult standard meals in the pediatric population. They also looked at the extension of this criterion to nonstandard cheese-based meals. In the cohort, 18% of the children ate partial meals and 7% ate an alternative cheese-based meal. Adult criteria were used to initially characterize the studies as normal or abnormal emptying. The authors showed data indicating no differences in classifying normal or abnormal gastric emptying comparing complete, partial, and alternate meal types across sexes and age groups. It is unethical and/or challenging to recruit normal pediatric subjects for such studies, so the authors used a data-driven clustering approach to independently verify the appropriateness of the adult criteria threshold. They showed good concordance between both methods of stratifying subjects with normal and delayed gastric emptying, further supporting the use of the adult criteria for pediatric use. They concluded that the adult criterion for normal gastric motility can be applied to children who ingest as little as 50% of the standard adult meal and that cheese-based meals offer viable alternatives to the full adult standard meal in the pediatric population. These data provide previously unavailable guidance for managing children who eat less than the full meal or an alternative meal (additionally useful as alternative meals become more common even in the adult population).

Maurer and colleagues from Temple University Hospital/Temple University School of Medicine (Philadelphia, PA) investigated the "Added value of small bowel transit scintigraphy for assessment of patients with symptoms of gastroparesis" [428]. The rationale for the research was that dyspeptic symptoms may be nonspecific and are often not correlated with the results of gastric emptying studies. The authors aimed to determine the prevalence of delayed small bowel transit in patients undergoing gastric emptying scintigraphy for symptoms of gastroparesis and to determine

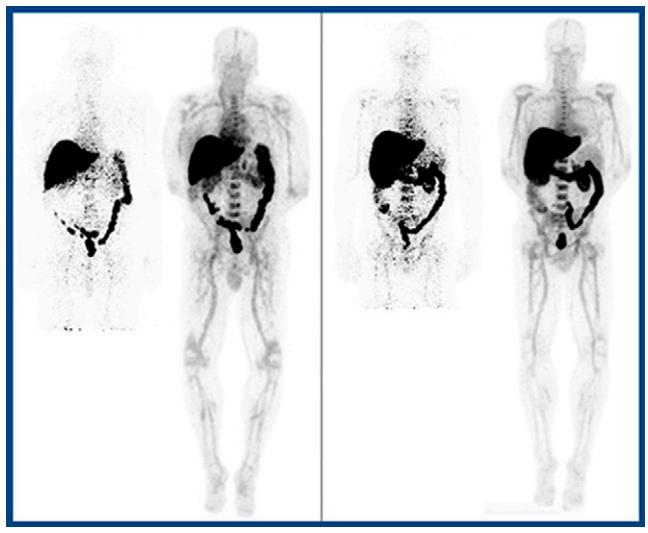

FIGURE 5. First-in-human total-body PET imaging of HIV with ^{89}Zr-VRC01 on the EXPLORER. Left: ^{89}Zr-VRC01 imaging with conventional PET (left) and the EXPLORER (right) in an antiretroviral therapy–suppressed patient (acquired at 72 hours after tracer injection). Right: ^{89}Zr-VRC01 imaging with conventional PET (left) and the EXPLORER (right) in a patient with low-level viremia. The difference in image quality between the 20-minute 1-bed position with the EXPLORER and the 30-minute 6-bed positions with a standard PET camera is clear.

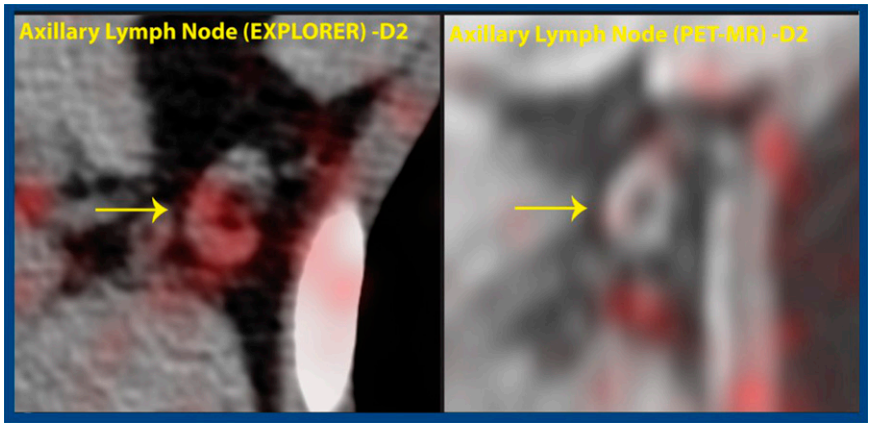

FIGURE 6. Total-body PET imaging of HIV with ^{89}Zr-VRC01 on the EXPLORER (left) showed increased axillary lymph node (arrows) 2 days after tracer injection compared with conventional PET/MR imaging (right). Increased soft tissue/blood ratios were also seen in patients with active viremia compared with those in patients with antiretroviral therapy suppression.

what symptoms are associated with delayed small bowel transit and the ways in which these differ from those associated with delayed gastric emptying. The investigation included 363 patients with evaluable studies who had undergone both a gastric emptying study and a small bowel transit study. Of these, 174 (47.9%) had delayed solid gastric emptying (>60% retention at 2 hours or >10% at 4 hours), 141 (38.8%) had delayed liquid gastric emptying (>50% retention at 1 hour), and 70 (19.3%) had delayed small bowel transit (<40% ^{111}In liquid activity reaching the terminal ileum or cecum/colon at 6 hours). Among those with delayed small bowel transit, 24 (6.6%) had isolated small bowel transit abnormalities and normal gastric emptying. Symptoms more commonly associated with isolated small bowel transit included postprandial fullness, stomach fullness, bloating, and visibly larger stomach, whereas those associated with delayed solid gastric emptying included more nausea and vomiting. The authors concluded that the addition of small bowel transit studies to gastric emptying scintigraphy may explain some of the symptoms of patients presenting with upper gastrointestinal dyspepsia and/or suspected gastroparesis. Many clinical sites do not perform small bowel transit studies because of the amount of time required, but these preliminary data suggest the potential for tailoring studies based on individual patient symptoms.

Development: New Tracers

Last year at the SNMMI Annual Meeting, a group of researchers presented their initial work on a novel radiotracer, ^{18}F-fluoride-alumina nanoparticles, to visualize mucociliary transport and clearance in a pig model, but translatability was limited as the agent had to be administered via an endotracheal tube. This year, the same team continued their work with the development of a radioaerosolized version of the nanoparticles. Akurathi et al. from the University of Iowa/University of Iowa Carver College of Medicine (Iowa City) reported on "Evaluation of lung mucociliary transport and clearance in ferrets: Imaging nebulized radioaerosols" [1490]. Their cystic fibrosis ferret model reflects the full spectrum of cystic fibrosis phenotypes observed in human patients. The ^{18}F-fluoride alumina nanoparticles (particle size ≤50 nm) had good clearance from the trachea during the initial phase of dosing (<5 minutes), faster than was seen

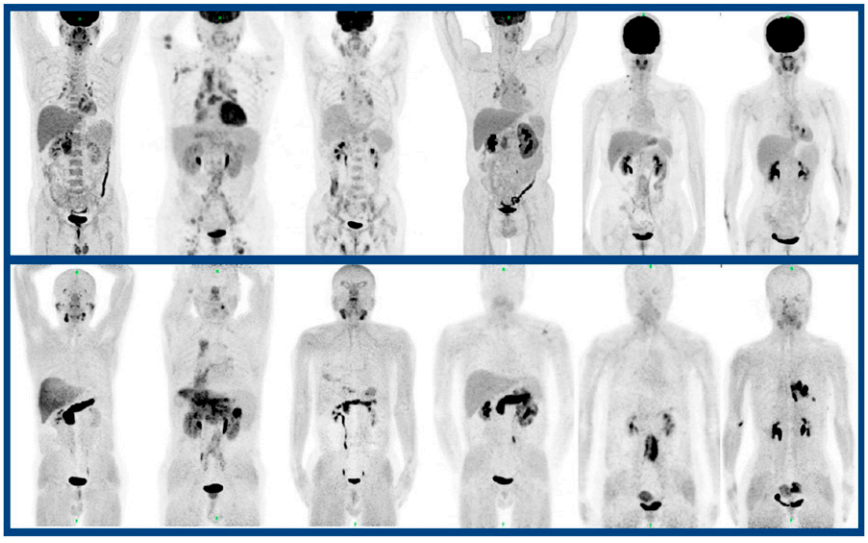

FIGURE 7. "^{68}Ga-FAPI PET/CT imaging of fibrosis in IgG4-related disease. Top row: ^{18}F-FDG PET/CT imaging in a series of 5 patients with IgG4-related disease. Bottom row: Corresponding ^{68}Ga-FAPI PET/CT images acquired in the same patients. ^{68}Ga-FAPI PET/CT showed a larger number of organs involved in about half of patients, with the most involvement identified in the pancreas, salivary glands, bile duct/liver, and lacrimal glands. ^{18}F-FDG uptake was higher in the lymph nodes, but this is associated with less morbidity. This work highlighted the ways in which different tracers can show varying aspects of disease, in this case organ vs. nodal involvement.

for the comparative ^{99m}Tc-sulfur colloid agent (particle size, 0.03–10 μm) (Fig. 4). The time–activity curve showed the rapid clearance of the ^{18}F-labeled nanoparticle. Given the imaging properties of ^{18}F and the ability to perform early dynamic PET/CT scanning, ^{18}F-fluoride-alumina nanoparticles have the potential for expanded studies in small animal cystic fibrosis models. The team's ultimate goal is to translate this imaging technique to patients with cystic fibrosis, particularly for monitoring response to therapy.

Exciting technology and tracers previously presented in oncology are making their way into general nuclear medicine applications. Beckford-Vera and colleagues from the University of California at San Francisco, the University of California at Davis, and the University of California Davis Medical Center (Sacramento) presented "First-in-human total-body PET imaging of HIV with ^{89}Zr-VRC01 on the EXPLORER" [545]. HIV can persist in anatomic reservoirs and rebound if successful antiretroviral therapy is stopped. The ability to assess this viral burden, however, remains a challenge. VRC01 is a broadly neutralizing monoclonal antibody that binds HIV envelope glycoprotein 120. Figure 5 compares images acquired with conventional PET/MR to images acquired with the EXPLORER, the first total-body PET/CT device. The image on the left is of an antiretroviral therapy–suppressed patient, and on the right is a patient with low-level viremia. The difference in image quality between the 20-minute 1-bed position with the EXPLORER and the 30-minute 6-bed positions with a standard PET camera is clear. Figure 6 shows increased sensitivity for detection of antibody uptake in a small node with the EXPLORER. Increased soft tissue/blood ratios were also seen in patients with active viremia compared with those in patients with antiretroviral therapy suppression. The authors concluded that "utilization of total-body imaging demonstrates the potential to inform on whole-body anatomical localization and burden of persistent HIV infection." The abilities of the total-body PET EXPLORER open up possibilities for the use of many tracers, such as antibody imaging, that have typically been more challenging in the past.

Luo et al. from Peking Union Medical College Hospital (Beijing, China) investigated "^{68}Ga-FAPI PET/CT for imaging of fibrosis in IgG4-related disease: Comparison to ^{18}F-FDG PET/CT" [544]. IgG4-related disease causes significant morbidity and mortality, primarily as the result of organ dysfunction from uncontrolled and progressing fibrosis. The diagnosis is based on serum IgG4 blood plasmablast concentration ratios, but these do not localize disease in a way that can guide tissue biopsy. The team studied 26 patients with both ^{18}F-FDG and ^{68}Ga-FAPI. ^{68}Ga-FAPI PET/CT showed a larger number of organs involved in about half of patients, with the most involvement identified in the pancreas, salivary glands, bile duct/liver, and lacrimal glands (Fig. 7). Of note, ^{68}Ga-FAPI uptake was higher in the pancreas and liver, organs in which progressing fibrosis could result in significant organ dysfunction and morbidity. ^{18}F-FDG uptake was higher in the lymph nodes, but this is associated with less morbidity.

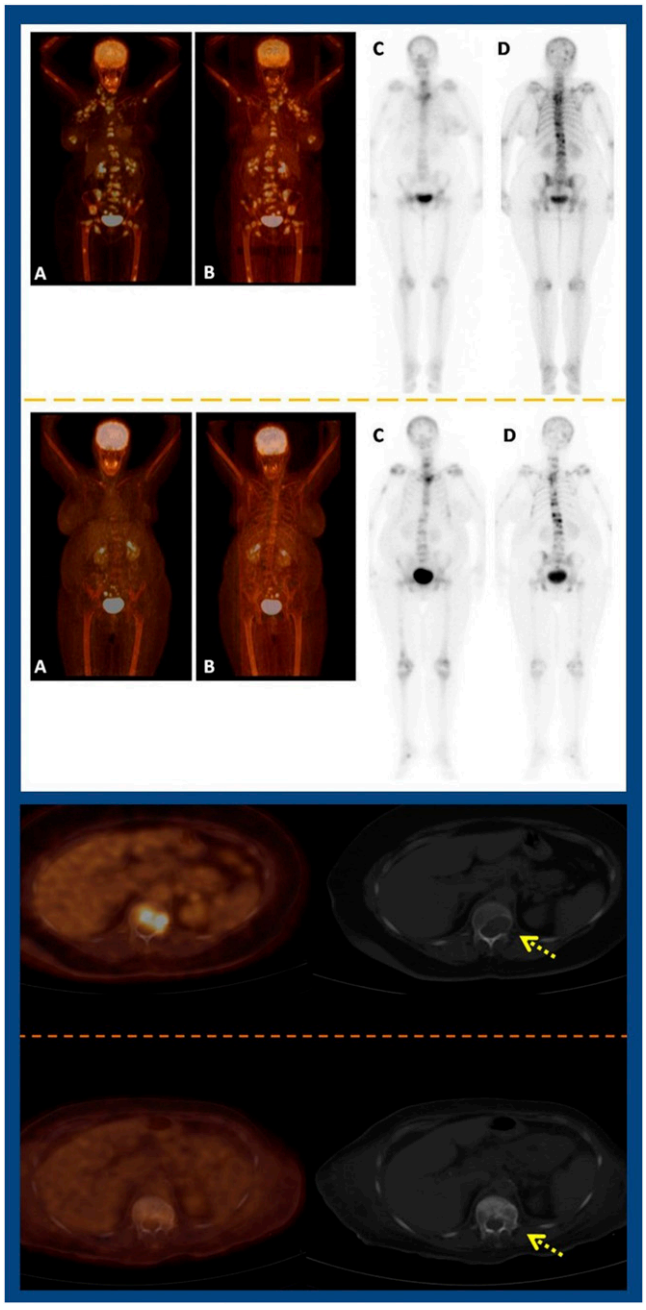

FIGURE 8. ^{18}F-FDG PET/CT and ^{99m}Tc-MDP bone scintigraphy in estimation of metastatic osseous burden in breast cancer patients. A semiquantitative metastatic osseous score based on PET was more closely correlated with changes in tumor and bone markers than bone scan score. Top, left block, top and bottom: ^{18}F-FDG PET/CT imaging in 2 patients before and after treatment. Middle block: Comparative ^{99m}Tc-MDP bone scintigraphy before and after treatment in the same patients. PET scores decreased but the bone scan scores remained the same. Bottom block: Example of an ^{18}F-FDG-avid lytic lesion that became non-FDG avid after treatment and was sclerotic on follow-up.

The authors concluded that ^{68}Ga-FAPI might be a promising imaging agent for assessment of IgG4-related disease. This work highlighted the ways in which different tracers can show

varying aspects of disease (in this case, organ vs. nodal involvement). Future studies investigating these agents must work to align clinical questions with clinically relevant endpoints.

I will end this summary with a disease setting seen every day in the nuclear medicine clinic: breast cancer bone metastases, where the question of bone scanning vs. ^{18}F-FDG PET is a growing focus. Nasr and colleagues from Cairo University Hospital (Egypt), Prince Sultan Military Medical City (Riyadh, Saudi Arabia), and Assuit University Hospital (Egypt) reported on the "Difference between ^{18}F-FDG PET/CT and ^{99m}Tc-methyl diphosphonate (^{99m}Tc-MDP) bone scintigraphy in estimation of metastatic osseous burden in breast cancer patients: A comparative study in view of CA15-3 and alkaline phosphatase" [609]. In 37 patients with breast cancer metastasized to bone, they showed (not surprisingly) that a semiquantitative metastatic osseous score based on ^{18}F-FDG PET was more closely correlated with changes in tumor and bone markers than a bone scan score. Comparative examples in Figure 8 show ^{18}F-FDG uptake throughout the bones. Although uptake is evident in the ^{99m}Tc-MDP bone scan, it does not have the same extent or detail as the PET/CT. After successful treatment in this study, PET scores decreased but the bone scan scores remained the same. Figure 8 also shows a classic example of an FDG-avid lytic lesion that became non-FDG-avid and sclerotic after treatment. The bone scan remains the go-to test in many clinics and clinical trials assessing response in metastatic breast cancer, but here we see an example of old bread-and-butter imaging concepts that we may not be optimizing to their fullest potential.

Conclusion

This is an exciting time in general nuclear medicine, with new and potentially transforming technologies and methods. We have seen here only a few examples of the outstanding work presented at this meeting. Going forward, we must be engaged and work closely with our clinical colleagues to demonstrate benefits in workflow and/or outcomes. I am optimistic that if we do this as a community, we can continue to advance general nuclear medicine.

COVID-19 and Ventilation/Perfusion (V/Q) Lung Studies

On August 28 SNMMI released updates to a previous statement responding to concerns regarding ventilation/perfusion (V/Q) lung scans and, specifically, the inherent risk of spread of COVID-19 to patients and staff from the ventilation portion of this study. At the time of the release of the original statement on March 19, many institutions opted not to perform ventilation studies. In the interim, the COVID-19 pandemic has evolved in different ways depending on institutions, locations, and populations, with questions about the timing and safety of resuming performance of the ventilation portion of V/Q studies.

The transmissibility of COVID-19 associated with medical ventilation systems has not yet been fully elucidated. In some situations, it may remain appropriate not to perform ventilation studies, for example, in institutions or practices in areas of high or increasing COVID-19 prevalence or where access to COVID-19 testing is inadequate.

The goal of the updated statement was to recognize that, in some regions and clinical situations, a ventilation study may be deemed to be clinically necessary to help diagnose lung disease, including vascular and airway disease. In these settings, performance of ventilation studies may be considered, with local and institutional COVID-19 policies and procedures for aerosol-generating and nonaerosolizing procedures serving as the primary source of guidance. The following considerations, which typically are included in facility policies and procedures, should be reviewed prior to performing ventilation studies:

1. In general, patients should have documentation of a negative COVID-19 polymerase chain reaction test; however, in some cases, local policies or regulations may be different.
2. Technologists should wear appropriate personal protective equipment (PPE) when performing ventilation studies, consistent with local policies for the performance of aerosol-generating and nonaerosolizing procedures.
3. Airflow in the room in which ventilation studies are performed should be evaluated, which may help determine the required time for room turnover after such studies.
4. The availability and administration feasibility of ventilation agents—including FDA-approved agents such as ^{99m}Tc-DTPA, ^{133}Xe gas, and other agents (e.g., ^{99m}Tc-labeled fine carbon particles or ^{99m}Tc-sulfur colloid)—should be considered for performance of ventilation studies.
5. It is recommended that local infection control groups be engaged for guidance and to help evaluate facilities, equipment, and staff PPE use for performing ventilation studies.
6. The approach to performing a ventilation scan in relation to the perfusion scan (i.e., ventilation then perfusion vs. perfusion then ventilation) should be considered on a case-by-case basis, depending on the clinical indication and in consultation with the referring physician.

SNMMI will continue to monitor the COVID-19 pandemic and provide updated information whenever possible.

SNMMI